

Neuron’s Eye View: Inferring Features of Complex Stimuli from Neural Responses

Xin (Cindy) Chen^{1,3}, Jeffrey M. Beck^{2,3}, John M. Pearson^{1,3*}

1 Duke Institute for Brain Sciences, Duke University, Durham, North Carolina, USA

2 Department of Neurobiology, Duke University Medical Center, Durham, North Carolina, USA

3 Center for Cognitive Neuroscience, Duke University, Durham, North Carolina, USA

* john.pearson@duke.edu

Abstract

Experiments that study neural encoding of stimuli at the level of individual neurons typically choose a small set of features present in the world — contrast and luminance for vision, pitch and intensity for sound — and assemble a stimulus set that systematically varies along these dimensions. Subsequent analysis of neural responses to these stimuli typically focuses on regression models, with experimenter-controlled features as predictors and spike counts or firing rates as responses. Unfortunately, this approach requires knowledge in advance about the relevant features coded by a given population of neurons. For domains as complex as social interaction or natural movement, however, the relevant feature space is poorly understood, and an arbitrary *a priori* choice of features may give rise to confirmation bias. Here, we present a Bayesian model for exploratory data analysis that is capable of automatically identifying the features present in unstructured stimuli based solely on neuronal responses. Our approach is unique within the class of latent state space models of neural activity in that it assumes that firing rates of neurons are sensitive to multiple discrete time-varying features tied to the *stimulus*, each of which has Markov (or semi-Markov) dynamics. That is, we are modeling neural activity as driven by multiple simultaneous stimulus features rather than intrinsic neural dynamics. We derive a fast variational Bayesian inference algorithm and show that it correctly recovers hidden features in synthetic data, as well as ground-truth stimulus features in a prototypical neural dataset. To demonstrate the utility of the algorithm, we also apply it to cluster neural responses and demonstrate successful recovery of features corresponding to monkeys and faces in the image set.

Introduction

The question of how the brain encodes information from the natural world forms one of the primary areas of study within neuroscience. For many sensory systems, particularly vision and audition, the discovery that single neurons modulate their firing of action potentials in response to particular stimulus features has proven foundational for theories

of sensory function. Indeed, neuronal responses to contrast, edges, and motion direction appear to form fundamental primitives on which higher-level visual abstractions are built. Nevertheless, many of these higher-level abstractions do not exist in a stimulus space with obvious axes. As a result, experimenters must choose *a priori* features of interest in constructing their stimulus sets, with the result that cells may appear weakly tuned due to misalignment of stimulus and neural axes.

For example, in vision, methods like reverse correlation have proven successful in elucidating response properties of some cell types, but such techniques rely on a well-behaved stimulus space and a highly constrained encoding model in order to achieve sufficient statistical power to perform inference [1–3]. However, natural stimuli are known to violate both criteria, generating patterns of neural activity that differ markedly from those observed in controlled experiments with limited stimulus complexity [3–5]. Information-based approaches have gone some way in addressing this challenge [4], but this approach assumes a metric structure on stimuli in order to perform optimization, and was recently shown to be strongly related to standard Poisson regression models [6].

More recently, Gallant and collaborators have tackled this problem in the context of fMRI, demonstrating that information present in the blood oxygen level-dependent (BOLD) signal is sufficient to classify and map the representation of natural movie stimuli across the brain [7–9]. These studies have used a number of modeling frameworks, from Latent Dirichlet Allocation for categorizing scene contents [9] to regularized linear regression [8] to sparse nonparametric models [7] in characterizing brain encoding of stimuli, but in each case, models were built on pre-labeled training data. Clearly, a method that could infer stimulus structure directly from neural data themselves could extend such work to less easily characterized stimulus sets like those depicting social interactions.

Another recent line of work, this one focused on latent Poisson processes, has addressed the task of modeling the low dimensional dynamics of neural populations [10–16]. Using generalized linear models and latent linear dynamical systems as building blocks, these models have proven able to infer (functional) connectivity [10], estimate spike times from a calcium images [11], and identify subgroups of neurons that share response dynamics [13, 15, 16]. Inference in these models is generally performed via expectation maximization, though [14–18] also used a variational Bayesian approach. Our work is distinct from those models, however, in that those were concerned with modeling and discriminating *internal* states based on neural responses, while this work focuses on detecting features in *external* stimuli. Moreover, in contrast to [13–16], we focus on multiple binary latent states as a means of “tagging” a finite number of overlapping stimulus features.

Our model sits at the intersection of these regression and latent variable approaches. We utilize a Poisson observation model that shares many of the same features as the commonly used generalized linear models for Poisson regression. We also assume that the latent features modulating neural activity are time-varying and Markov. However, we make 3 additional unique assumptions: First, we assume that the activity of each neuron is modulated by a combination of multiple independent latent features governed by (semi-)Markov dynamics. This allows for latents to evolve over multiple timescales with non-trivial duration distributions, much like the hand-labeled features in social interaction data sets. Second, we assume that these latents are tied to stimulus presentation. That is, when identical stimuli are presented, the same latents are also present. This allows us to model the dynamics of latent features of the *stimulus* that drive neural activity,

rather than intrinsic neural dynamics. Finally, we enforce a sparse hierarchical prior on modulation strength that effectively limits the number of latent features to which the population of neurons is selective. This allows for a parsimonious explanation of the firing rates of single units in terms of a small set of stimulus features. Finally, we perform full variational Bayesian inference on all model parameters and take advantage of conditional conjugacy to generate coordinate ascent update rules, nearly all of which are explicit. Combined with forward-backward inference for latent states, our algorithm is exceptionally fast, automatically implements Occam’s razor, and facilitates proper model comparisons using the variational lower bound.

Model

Observation model

Consider a population of U spiking neurons or units exposed to a series of stimuli indexed by a time index $t \in \{1 \dots T\}$. We assume that this time index is unique across all stimuli, such that a particular t represents a unique moment in a particular stimulus. In order to model repeated presentations of the same stimulus to the same neuron, we further assume that each neuron is exposed to a stimulus M_{tu} times, though we do not assume any relationship among M_{tu} . That is, we need not assume either that all neurons see each stimulus the same number of times, nor that each stimulus is seen by all neurons. It is thus typical, but not required, that M_{tu} be sparse, containing many 0s, as shown in Figure 1.

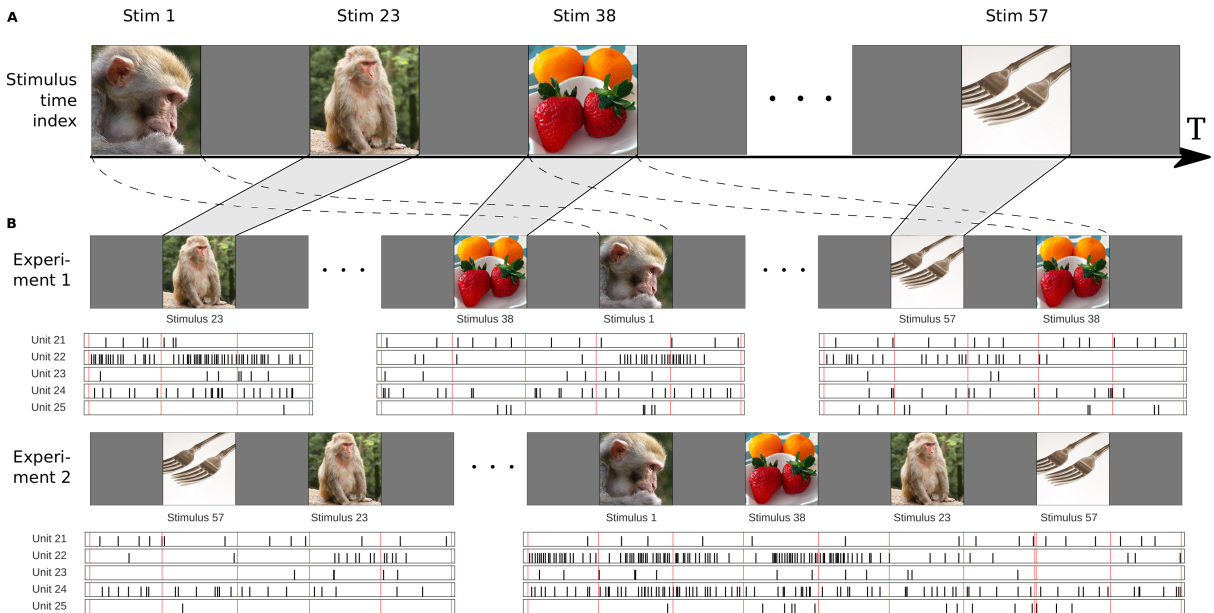


Fig 1. Observational model.

A: Stimuli are concatenated to form a single time series indexed by t . B: Individual experimental sessions draw from the available set of stimuli, with index m representing unique $(time, unit)$ presentations. Example stimulus sequences for two experiments are shown, with corresponding neuronal spike data. Note that the number of exposure times M_{tu} for each stimulus and unit can be different.

For each observation m in M_{tu} , we then observe a spike count, N_m . Note that m is a unique $(time, unit)$ pair that can be denoted by $(t(m), u(m))$. We model these spike counts

as arising from a Poisson process with time-dependent rate Λ_{tu} and observation-specific multiplicative overdispersion θ_m :

$$N_m \sim \text{Pois}(\Lambda_{t(m),u(m)}\theta_m) \quad \text{where } \theta_m \sim \text{Gamma}(s_{u(m)}, s_{u(m)}) \quad (1)$$

That is, for a given stimulus presentation, the spiking response is governed by the firing rate Λ , specific to the stimulus and unit, along with a moment-by-moment noise in the unit’s gain, θ_m . We restrict these θ_m to follow a Gamma distribution with the same shape and rate parameters, since this results in an expected noise gain of 1. In practice, we model this noise as independent across observations, though it is possible to weaken this assumption, allowing for θ_m to be autocorrelated in time (see Supplement). Note that both the unit and time are functions of the observation index m , and that the distribution of the overdispersion for each observation may be specific to the unit observed.

Firing rate model

At each stimulus time t , we assume the existence of K binary latent states z_{tk} and R observed covariates x_{tr} . The binary latent states can be thought of as time-varying “tags” of each stimulus — for example, content labels for movie frames — and are modeled as Markov chains with initial state probabilities π_k and transition matrices A_k . The observed covariates, by contrast, are known to the experimenter and may include contrast, motion energy, or any other *a priori* variable of interest.

We further assume that each unit’s firing rate at a particular point in time can be modeled as arising from the product of three effects: (1) a baseline firing rate specific to each unit (λ_0), (2) a product of responses to each latent state (λ_z), and (3) a product of responses to each observed covariate (λ_x):

$$\Lambda_{tu} = \lambda_{0u} \prod_{k=1}^K (\lambda_{zuk})^{z_{tk}} \prod_{r=1}^R (\lambda_{xur})^{x_{tr}} \quad (2)$$

Note that this is conceptually similar to the generalized linear model for firing rates (in which we model $\log \Lambda$) with the identification $\beta = \log \lambda$. However, by modeling the firing rate as a product and placing Gamma priors on the individual effects, we will be able to take advantage of closed-form variational updates resulting from conjugacy that avoid explicit optimization (see below). Note also, that because we assume the z_{tk} are binary, the second term in the product above simply represents the cumulative product of the gain effects for those features present in the stimulus at a given moment in time.

In addition, to enforce parsimony in our feature inference, we place sparse hierarchical priors with hyperparameters $\gamma = (c, d)$ on the λ_z terms:

$$\lambda_{zuk} \sim \text{Gamma}(c_{zk}, c_{zk}d_{zk}) \quad c_{zk} \sim \text{Gamma}(a_{ck}, b_{ck}) \quad d_{zk} \sim \text{Gamma}(a_{dk}, b_{dk}) \quad (3)$$

That is, the population distribution for the responses to latent features is a gamma distribution, with parameters that are themselves gamma-distributed random variables. As a result, $\mathbb{E}[\lambda_u] = d^{-1}$ and $\text{var}[\lambda_u] = (cd^2)^{-1}$, so in the special case of c large and $d \sim \mathcal{O}(1)$, the prior for firing rate response to each latent feature will be strongly concentrated around gain 1 (no effect). As we show below, this particular choice results in a model that only infers features for which the data present strong evidence, controlling for spurious feature detection. In addition, this particular choice of priors leads to closed-form

updates in our variational approximation. For the baseline terms, λ_{0u} , we use a non-sparse version of the same model; for the covariate responses, λ_{xu} , we model the unit effects non-hierarchically, using independent Gamma priors for each unit.

Putting all this together, we then arrive at the full generative model:

$$p(N, \Lambda, \theta) = p(N|\Lambda, \theta)p(\Lambda|\lambda, z)p(\lambda|\gamma)p(\gamma)p(z|A, \pi)p(A)p(\pi)p(\theta|s)p(s) \quad (4)$$

$$\text{where } p(\lambda|\gamma) = \prod_u p(\lambda_{0u}|c_0, d_0) \prod_{kr} p(\lambda_{zuk}|c_{zk}, d_{zk})p(\lambda_{xur}) \quad (5)$$

$$\text{and } p(\gamma) = p(c_0)p(d_0) \prod_k p(c_{zk})p(d_{zk}) \quad (6)$$

in conjunction with the definitions of $p(N|\Lambda, \theta)$ and $\Lambda(\lambda, z, x)$ in Eq (1) and (2). The generative model for spike counts is illustrated in Figure 2.

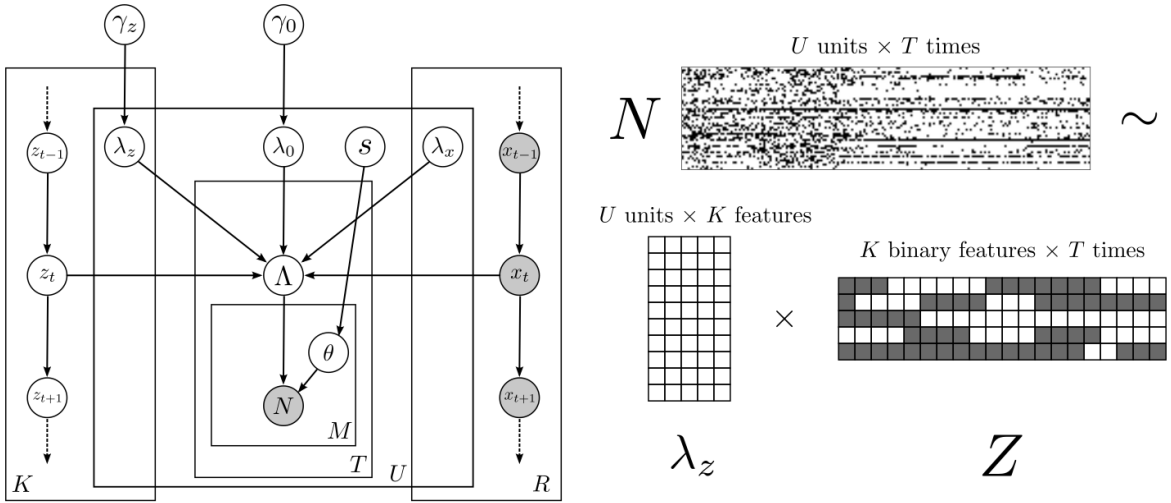


Fig 2. Generative model for spike counts.

A: Counts are assumed Poisson-distributed, with firing rates Λ that depend on each unit's responses (λ) to both latent discrete states z_t and observed covariates x_t that change in time, as well as a baseline firing rate λ_0 . γ nodes represent hyperparameters for the firing rate effects. θ is a multiplicative overdispersion term specific to each observation, distributed according to hyperparameters s . B: Spike counts N are observed for each of U units over stimulus time T for multiple presentations M_{tu} .

Inference

Given a sequence of stimulus presentations $(t(m), u(m))$ and observed spike counts N_m , we want to infer both the model parameters $\Theta = (\lambda_0, \lambda_z, \lambda_x, A, \pi, c_0, d_0, c_z, d_z, s)$ and latent variables $Z = (z_{kt}, \theta_m)$. That is, we wish to calculate the joint posterior density:

$$p(\Theta, Z|N) \propto p(N|Z, \Theta)p(Z)p(\Theta) \quad (7)$$

In general, calculating the normalization constant for this posterior is computationally intractable. Instead, we will use a variational approach, approximating $p(\Theta, Z|N)$ by a variational posterior $q(Z, \Theta) = q_Z(Z)q_\Theta(\Theta)$ that factorizes over parameters and latents but

is nonetheless close to p as measured by the Kullback-Leibler divergence [19]. Equivalently, we wish to maximize the variational objective

$$\mathcal{L} \equiv \mathbb{E}_q \left[\log \frac{p(\Theta, Z|N)}{q(\Theta, Z)} \right] = \mathbb{E}_q [\log p(\Theta, Z|N)] + \mathcal{H}[q_\Theta(\Theta)] + \mathcal{H}[q_Z(Z)] \quad (8)$$

with \mathcal{H} the entropy. We adopt the factorial HMM trick of [20], making the reasonable assumption that the posterior factorizes over each latent time series $z_{\cdot k}$ and the overdispersion factor θ_m , as well as the rate parameters $\lambda_{\cdot u}$ associated with each Markov process. This factorization results in a variational posterior of the form:

$$q(\Theta, Z) = q(c_0)q(d_0) \prod_m q(\theta_m) \prod_u q(s_u)q(\lambda_{0u}) \prod_r q(\lambda_{xur}) \times \prod_k q(c_k)q(d_k)q(\lambda_{zuk})q(c_{zk})q(d_{zk})q(z_k)q(\pi_k)q(A_k) \quad (9)$$

With this ansatz, the variational objective decomposes in a natural way, and choices are available for nearly all of the qs that lead to closed-form updates.

Variational posterior

From Eq (1) and (2) above, we can write the probability of the observed data N as

$$\begin{aligned} \log p(N, z|x, \Theta) &= \sum_{mkr} [N_m (\log \theta_m + \log \lambda_{0u(m)} + z_{t(m)k} \log \lambda_{zu(m)k} + x_{t(m)r} \log \lambda_{xu(m)r})] \\ &\quad - \sum_m \theta_m \Lambda_{t(m)u(m)} + \sum_{mk} \log(A_k)_{z_{t(m)+1,k}, z_{t(m),k}} + \sum_k \log(\pi_k)_{z_{0k}} + \text{constant}, \quad (10) \end{aligned}$$

where again, m indexes observations of $(t(m), u(m))$ pairs and the last two nontrivial terms represent the probability of the Markov sequence given by z_{tk} . Given that Eq (10) is of an exponential family form for θ and λ when conditioned on all other variables, free-form variational arguments [19] suggest variational posteriors:

$$\lambda_{0u} \sim \text{Gamma}(\alpha_{0u}, \beta_{0u}) \quad \lambda_{zuk} \sim \text{Gamma}(\alpha_{zuk}, \beta_{zuk}) \quad \lambda_{xur} \sim \text{Gamma}(\alpha_{xur}, \beta_{xur}) \quad (11)$$

For the first of these two, updates in terms of sufficient statistics involving expectations of $\gamma = (c, d)$ are straightforward (see Supplement). However, this relies on the fact that $z_t \in \{0, 1\}$. The observed covariates x_t follow no such restriction, which results in a transcendental equation for the β_x updates. In our implementation of the model, we solve this using an explicit BFGS optimization on each iteration. Moreover, we place non-hierarchical Gamma priors on these effects: $\lambda_{xur} \sim \text{Gamma}(a_{xur}, b_{xur})$.

As stated above, for the latent states and baselines, we assume hierarchical priors. This allows us to model each neuron's firing rate response to a particular stimulus as being drawn from a population response to that same stimulus. We also assume that the moment-to-moment noise in firing rates, θ_m , follows a neuron-specific distribution. As a result of the form of this hierarchy given in Eq (3), the first piece in Eq (8) contains multiple terms of the form

$$\mathbb{E}_q \left[\sum_u \log p(\lambda_u | c, d) \right] = \sum_u \mathbb{E}_q [(c-1) \log \lambda_u - cd \lambda_u + c \log cd - \log \Gamma(c)] \quad (12)$$

In order to calculate the expectation, we make use of the following inequality [21]

$$\sqrt{2\pi} \leq \frac{z!}{z^{z+\frac{1}{2}}e^{-z}} \leq e \quad (13)$$

to lower bound the negative gamma function and approximate the above as

$$\log p(\lambda) \geq \sum_u \left[(c-1)(\log \lambda_u + 1) - cd\lambda_u + c \log d + \frac{1}{2} \log c \right] \quad (14)$$

Clearly, the conditional probabilities for c and d are gamma in form, so that if we use priors $c \sim \text{Gamma}(a_c, b_c)$ and $d \sim \text{Gamma}(a_d, b_d)$ the posteriors have the form

$$c \sim \text{Gamma} \left(a_c + \frac{U}{2}, b_c + \sum_u \mathbb{E}_q [d\lambda_u - \log \lambda_u - \log d - 1] \right) \quad (15)$$

$$d \sim \text{Gamma} \left(a_d + U\mathbb{E}_q[c], b_d + \sum_u \mathbb{E}_q[c\lambda_u] \right) \quad (16)$$

This basic form, with appropriate indices added, gives the update rules for the hyperparameter posteriors for λ_0 and λ_z . For θ , we simply set $c = s_u$ and $d = 1$.

For each latent variable z , the Markov Chain parameters π_k and A_k , together with the observation model Eq (10) determine a Hidden Markov Model, for which inference can be performed efficiently via conjugate updates and the well-known forward-backward algorithm [22]. More explicitly, given π , A , and the emission probabilities for the observations, $\log p(N|z)$, the forward-backward algorithm returns the probabilities $p(z_t = s)$ (posterior marginal), $p(z_{t+1} = s', z_t = s)$ (two-slice marginal) and $\log Z$ (normalizing constant).

Experiments

Synthetic data

We generated synthetic data from the model for $U = 100$ neurons for $T = 10,000$ time bins of $dt = 0.0333s$ (≈ 6 min of movie at 30 frames per second). Assumed firing rates and effect sizes were realistic for cortical neurons, with mean baseline rates of 10 spikes/s and firing rate effects given by a $\text{Gamma}(1, 1)$ distribution for $K_{\text{data}} = 3$ latent features. In addition, we included $R = 3$ known covariates generated according to Markov dynamics. For this experiment, we assumed that each unit was presented only once with the stimulus time series, so that $M_{tu} = 1$. That is, we tested a case in which inference was driven primarily by variability in population responses across stimuli rather than pooling of data across repetitions of the same stimulus. Moreover, to test the model's ability to parsimoniously infer features, we set $K = 5$. That is, we asked the model to recover more features than were present in the data. Finally, we placed hierarchical priors on neurons' baseline firing rates and sparse hierarchical priors on firing rate effects of latent states. We used 10 random restarts and iterated over parameter updates until the fractional change in \mathcal{L} dropped below 10^{-4} .

As seen in Figure 3, the model correctly recovers only the features present in the original data. We quantified this by calculating the normalized mutual information $\hat{I} \equiv I(X, Y) / \sqrt{H(X)H(Y)}$, between the actual states and the inferred states, with $H(Z)$

and I estimated by averaging the variational posteriors (both absolute and conditioned on observed states) across time. Note that superfluous features in the model have high posterior uncertainty for z_k and high posterior confidence for λ_{z_k} around 1 (no effect). In addition, the model correctly recovers coefficients for the observed covariates, and when limited to fewer features than in the generating model, recovers a subset of the features accurately rather than blending features together (Figure 3).

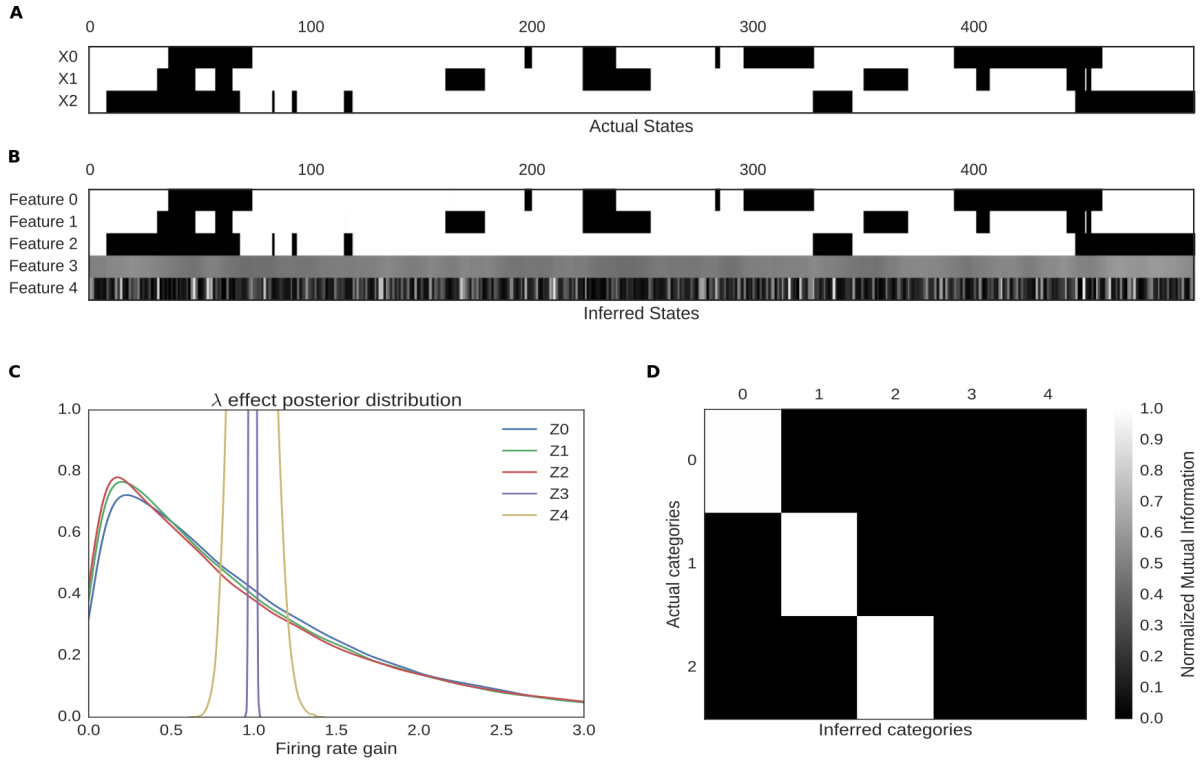


Fig 3. Comparison of actual and inferred states of the synthetic data.

A: Actual features for a subset of stimulus times in the synthetic dataset. B: Recovered binary features for the same subset. Features have been reordered for display. The unused features are in gray, indicating a high posterior uncertainty in the model. C: Population posterior distributions for inferred hyper parameters. Features 3 and 4 are effectively point masses around gain 1 (no effect), while features 1–3 approximate the Gamma(1, 1) data-generating model. D: Normalized mutual information between actual and inferred states.

Labeled neural data

We applied our model to a well-studied neural data set comprising single neuron recordings from macaque area LIP collected during the performance of a perceptual discrimination task [23]¹. In the experiment, stimuli consisted of randomly moving dots, some percentage of which moved coherently in either the preferred or anti-preferred direction of motion for each neuron. The animal’s task was to report the direction of motion. Thus, in addition to 5 coherence levels, each trial also varied based on whether the motion direction corresponded to the target in or out of the response field as depicted in Fig. 4.²

¹Data available at <https://www.shadlenlab.columbia.edu/resources/RoitmanDataCode.html>

²In the case of 0% coherence, the direction of motion was inherently ambiguous and coded according to the monkey’s eventual choice.

We fit a model with $K = 10$ features and $U = 27$ units to neural responses from the 1-second stimulus presentation period of the task. Spike counts corresponded to bins of $dt = 20\text{ms}$. For this experiment, units were individually recorded, so each unit experienced a different number of presentations of each stimulus condition, implying a ragged observation matrix. As a result, this dataset tests the model’s ability to leverage shared task structure across multiple sessions of recording, demonstrating that simultaneously recorded units are not required for inference of latent states.

Figure 4 shows the experimental labels from the concatenated stimulus periods, along with labels inferred by our model. Once again, the model has left some features unused, but correctly discerned differences between stimuli in the unlabeled data. Even more importantly, though given the opportunity to infer ten distinct stimulus classes, the model has made use of only five. Moreover, the discovered features clearly recapitulate the factorial design of the experiment, with the two most prominent features, Z_1 and Z_2 , capturing complementary values of the variable with the largest effect in the experiment: whether or not the relevant target was inside our outside the receptive field of the recorded neuron. This difference can be observed in both the averaged experimental data and the predicted data from the model (see Figure 4.C), where the largest differences are between the dotted and solid lines.

But the model also reproduces less obvious features: it correctly discriminates between two identical stimulus conditions (0% coherence) based on the monkey’s eventual decision (In vs Out). In addition, the model correctly captures the initial 200ms “dead time” during the stimulus period, in which firing rates remain at pre-stimulus baseline. (Note that the timing is locked to the stimulus and consistent across trials, not idiosyncratic to each trial as in [24].) Finally, the model resists detection of features with little support in the experimental data. For instance, while feature Z_4 captures the large difference between 50% coherence and other stimuli, the model does not infer a difference between intermediate coherence levels that are indistinguishable in this particular dataset. That is, mismatches between ground truth labels and model-inferred features here reflect underlying ambiguities in the neural data, while the model’s inferred features correctly pick out those combinations of variables most responsible for differences in spiking across conditions.

Visual category data

As a second test of our model, we applied our algorithm to a designed structured stimuli dataset comprising $U = 56$ neurons from macaque inferotemporal cortex [25]. These neurons were repeatedly presented with 96 stimuli comprising 8 categories ($M = 1483$ total trials, with each stimulus exposed between 12 to 19 times to each unit) comprising monkey faces, monkey bodies, whole monkeys, natural scenes, food, manmade objects, and patterns (Figure 5.A). Data consisted of spike time series, which we binned into a 300ms pre-stimulus baseline, a 300ms stimulus presentation period, and a 300ms post-stimulus period. Three trials were excluded because of the abnormal stimulus presentation period. To maximize interpretability of the results, we placed strong priors on the π_k to formalize the assumption that all features were off during the baseline period. We also modeled overdispersion with extremely weak priors to encourage the model to attribute fluctuations in firing to noise in preference to feature detection. We again fit $K = 10$ features with sparse hierarchical priors on population responses.

The inferred categories based on binned population responses are shown in Figure

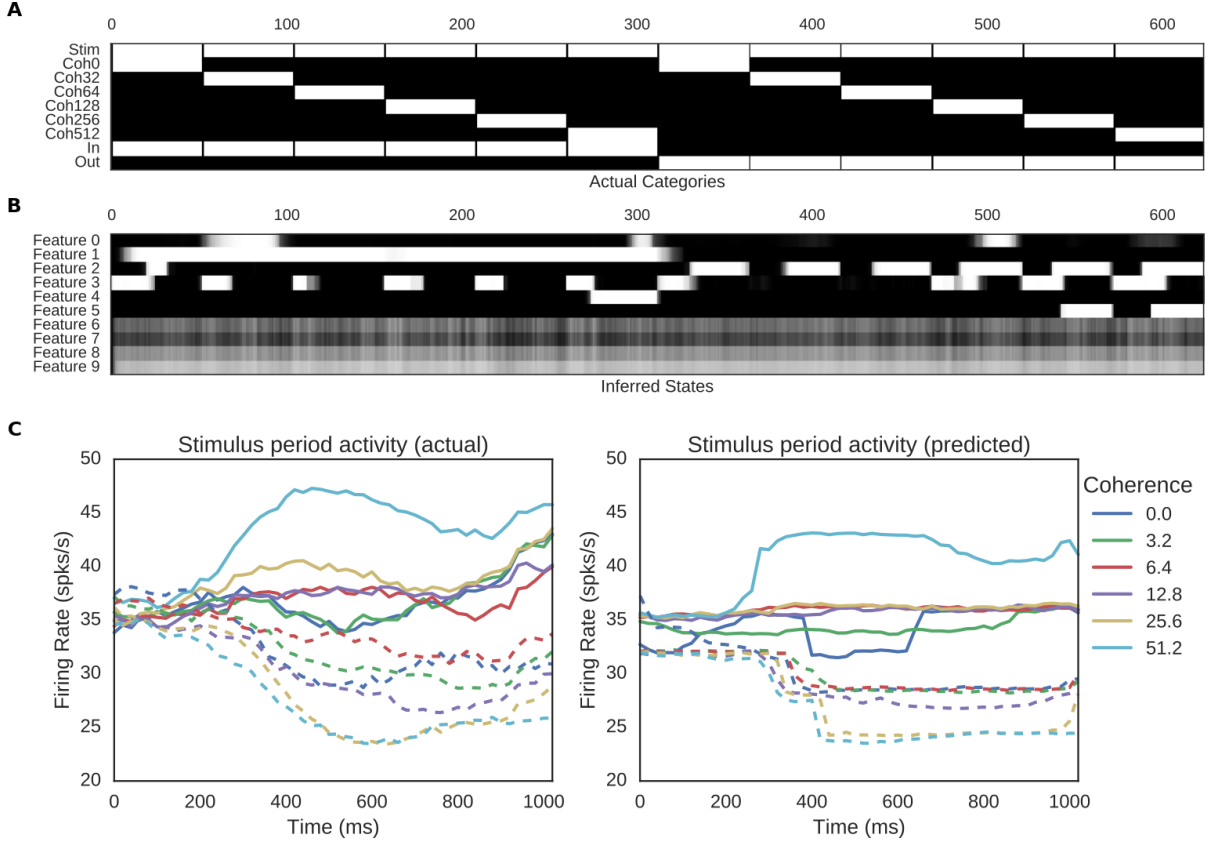


Fig 4. Comparison of actual and inferred states of the Roitman dataset.

A: Indicators of actual categories represented in the stimulus presentation period. The categories are not independent of each other. Stimuli are joined sequentially, labeled by a single, unique stimulus time. B: Recovered binary features during the stimulus presentation period. Note that model features 6 – 9 are unused and that Features 1 & 2 closely track the In and Out features of the data, respectively. C: Actual and predicted firing rates for the stimulus period. Note that the model infers stimulus categories from the data, including appropriate timing of differentiation between categories.

5.B. For clarity, in Figure 5, we only show population mean effects with a “> 5% gain” modulation sorted from the highest to the lowest, though the full set of inferred states can be found in Figure 6. Out of the original categories, our model successfully recovers three features clearly corresponding to categories involving monkeys (Features 0 – 2). These can be viewed additively, with Feature 0 exclusive to monkey face close-ups, Feature 1 any photo containing a monkey face, either near or far; and Feature 2 any image containing a monkey body part (including faces); but as we will argue, given the nature of the model, it may be better to view these as a “combinatorial” code, with monkey close-ups encoded as 0&1&2 (~ 59.46% increase in firing), whole monkeys as 1&2 (~ 32.47% increase), and monkey body parts as 2 (~ 7.62% increase). Of course, this is consistent with what was found in [25], though our model used no labels on the images. And our interpretation that these neurons are sensitive to close-ups and faraway face and body parts is consistent with findings by another study using different experimental settings [26].

Again, as noted above, our results in Figure 5.A and 5.B indicate predicted population responses, derived from the hierarchical prior. As evidenced in Figure 5.C and 5.D, individual neuron effects could be much larger. These panels show data for two example units, along with the model’s prediction. Clearly, the model recapitulates the largest

distinctions between images in the data, though the assumption that firing rates should be the same for all images with similar features fails to capture some variability in the results. Even so, uncertainties in the predicted firing rates are also in line with uncertainties from those of observed rates, indicating that our model is correctly accounting for trial-to-trial noise.

Finally, even the weaker, sparser features inferred by our model captured intriguing additional information. As shown in Figure 6, Feature 4, a feature only weakly present in the population as a whole (and thus ignored in 6.A), when combined with the stronger Features 0, 1, and 2, successfully distinguishes between the monkey close-ups with direct and averted gaze. (Stimulus 5, with averted gaze, is additionally tagged with Feature 5, which we view as an imperfect match.) Thus, despite the fact that Feature 4 is barely a 3.4% gain change over the population, it suggests a link between neural firing and gaze direction, one for which there happens to be ample evidence [27, 28]. Similarly, Feature 5, barely a 1.1% effect, correctly tags three of the four close-ups with rightward gaze (with one false positive). Clearly, neither of these results is dispositive in this particular dataset, but in the absence of hypotheses about the effect of head orientation and gaze on neuronal firing, these minor features might suggest hypotheses for future experiments.

An additional feature of our approach is that the generated labels provide a concise and fairly complete summary of the stimulus-related activity of all neural recordings, which can be observed by comparing the categorization performance of decoded neural activity to the categorization performance of the decoded features. Although our model is not a data compression method, it nonetheless preserves most of the information about image category contained in the $N = 56$ dimensional spike counts via a 10-dimensional binary code. That is, using a sparse logistic regression on two-bit and three-bit combinations of our features to predict stimulus category ties and outperforms, respectively a multinomial logistic regression on the raw spike counts (see Supplement).

Discussion

Here, we have proposed and implemented a method for learning features in stimuli via the responses of populations of spiking neurons. This work addresses a growing trend in systems neuroscience — the increasing use of rich and unstructured or structured stimulus sets — without requiring either expert labeling or a metric on the stimulus space. As such, we expect it to be of particular use in disciplines like social neuroscience, olfaction, and other areas in which the real world is complex and strong hypotheses about the forms of the neural code are lacking. By learning features of interest to neural populations directly from neural data, we stand to generate unexpected, more accurate (less biased) hypotheses regarding the neural representation of the external world.

Here, we have validated this method using structured, labeled stimuli more typical of neuroscience experiments, showing that our model is capable of parsimoniously and correctly inferring features in the low signal-to-noise regime of cortical activity, even in the case of independently recorded neurons. Furthermore, by employing a fully variational, Bayesian approach to inference, we gain three key advantages: First, we gain the advantages of Bayesianism in general: estimates of confidence in inferences, parsimony and regularization via priors, and the ability to do principled model comparison. Second, variational methods scale well to large datasets and can be easily parallelized when combining data from multiple recording sessions. Finally, variational methods are fast, in

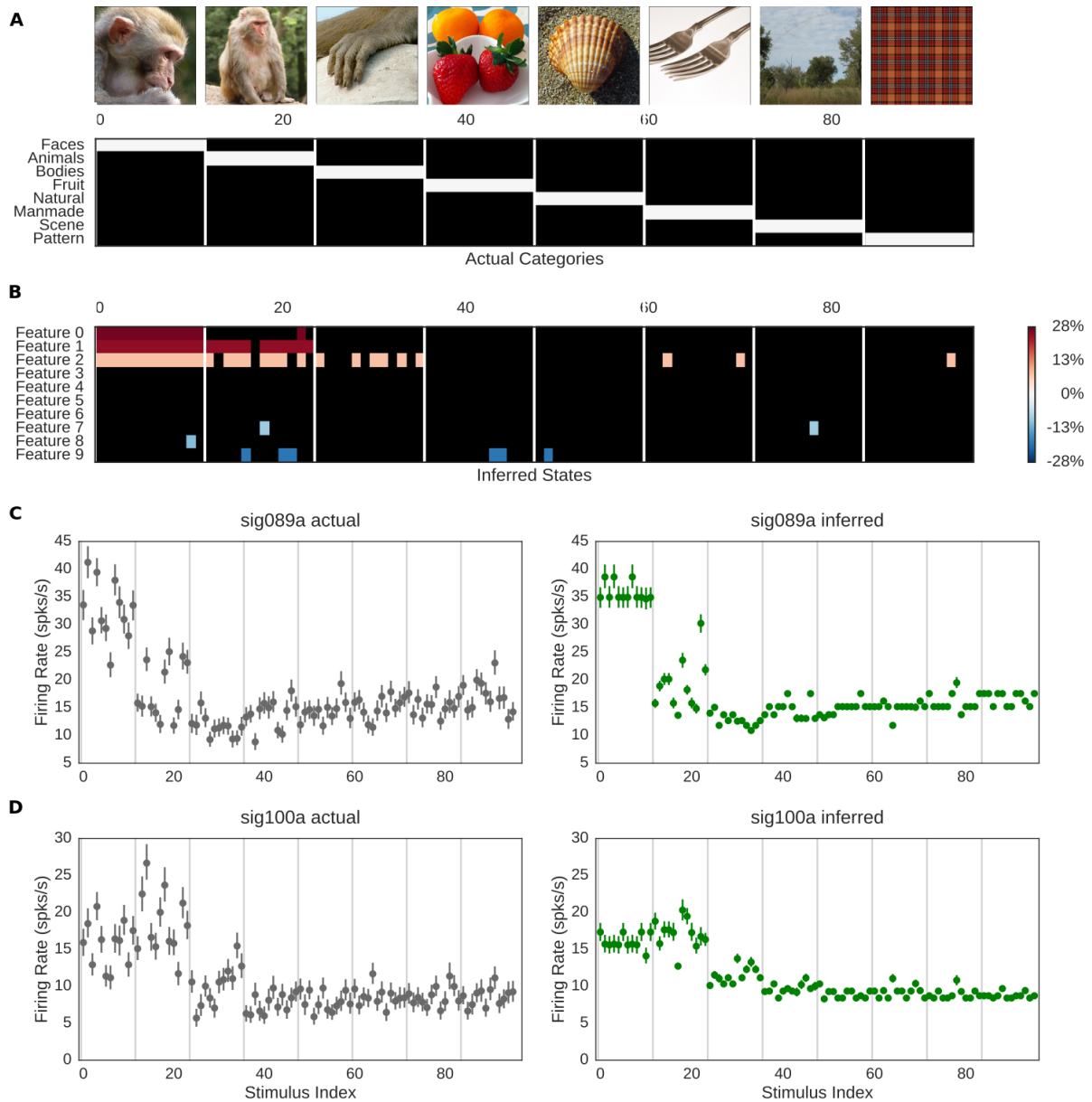


Fig 5. Comparison of actual and inferred states of the macaque dataset.

A: Actual categories in the macaque data set. 96 stimuli comprising 8 categories were presented in 1483 trials, with each stimulus presented to each neuron ~ 15 times. B: The inferred states from our model. The color represents the multiplicative effect to the population baseline firing rates. Note that our model shows a clear increase of firing rates in the categories of monkey faces, whole monkeys, and some stimuli within monkey bodies. C: Actual and predicted spikes per second across all stimulus of neuron 089a. D: Actual and predicted spikes per second across all stimulus of neuron 100a. Error bars for data represent 95% credible intervals for the firing rate based on observed data under a Poisson model with weak priors. Error bars on predictions are 95% credible intervals based on simulation from the approximate posterior for the given unit.

that they typically converge within only a few tens of iterations and in many case (such as ours) require mostly simple coordinate updates.

Finally, even small features in our model recapitulated known physiological results regarding face encoding in single neurons. And while these features alone might not

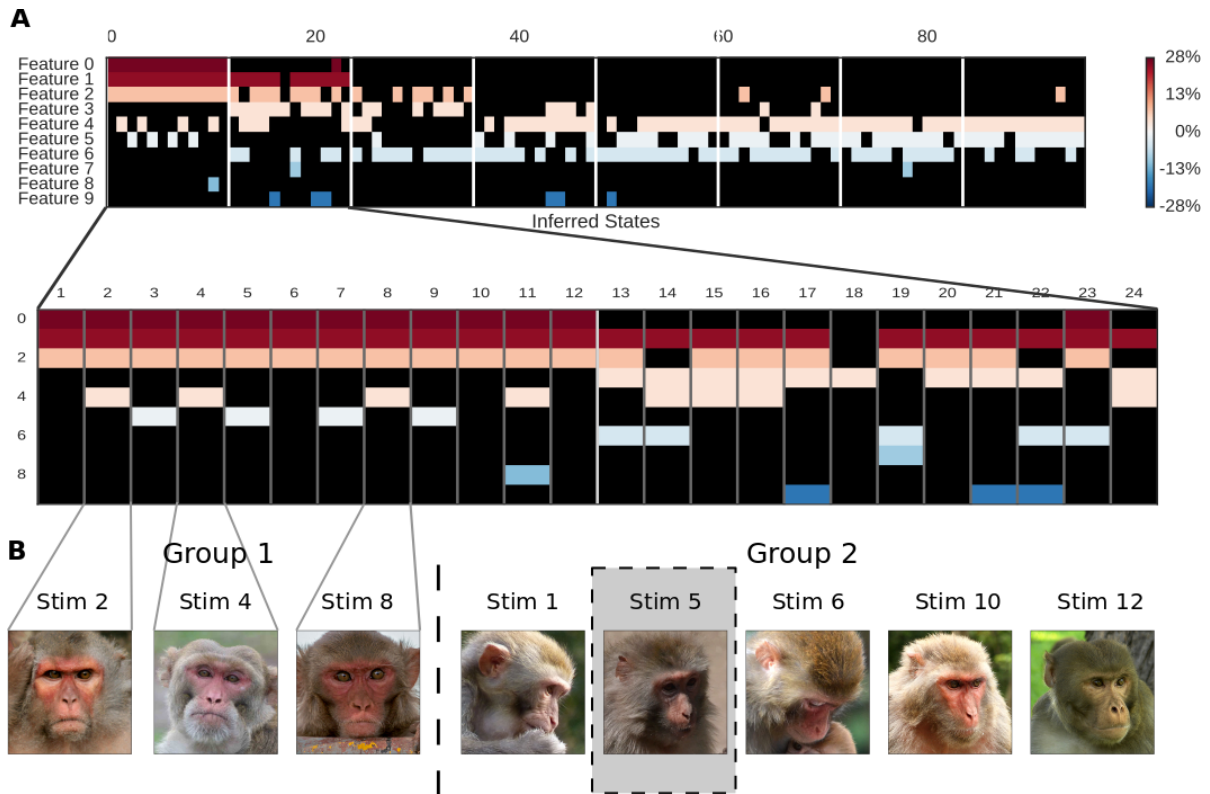


Fig 6. Small features suggest additional neural hypotheses.

A: Zoomed-in view of Figure 5.A, focusing on the first 24 images. B: The feature combinations 0&1&2 (Group 1) and 0&1&2&4 (Group 2) are distinguished by direct vs. indirect gaze. Stimulus 5, which is coded 0&1&2&5, may be considered a false negative.

provide proof positive of, e.g., viewpoint tuning, similar findings would be valuable in generating hypotheses in cases where the stimulus space and its neural correlates remain poorly understood. Thus our model facilitates an iterative experimental process: subjects are first be exposed to large, heterogeneous data; stimuli are then tagged based on neural responses; and finally, features with the largest effects are used to refine the set until it most accurately represents those stimuli with the largest neural correlates. Combined with the modularity of this and similar approaches, such models provide a promising opportunity to “build out” additional features that will meet the challenges of the next generation of experimental data.

Acknowledgments

We would like to thank David McMahan and David Leopold for generously sharing the visual category stimuli and neural data from [25] and for comments on the manuscript.

References

1. Steveninck RDRV, Bialek W. Real-Time Performance of a Movement-Sensitive Neuron in the Blowfly Visual System: Coding and Information Transfer in Short Spike Sequences. *Proceedings of the Royal Society of London B: Biological Sciences*. 1988;234(1277):379–414. doi:10.1098/rspb.1988.0055.

2. Ringach D, Shapley R. Reverse correlation in neurophysiology. *Cognitive Science*. 2004;28(2):147–166.
3. Ringach DL, Hawken MJ, Shapley R. Receptive field structure of neurons in monkey primary visual cortex revealed by stimulation with natural image sequences. *Journal of vision*. 2002;2(1):2.
4. Sharpee T, Rust NC, Bialek W. Analyzing neural responses to natural signals: maximally informative dimensions. *Neural computation*. 2004;16(2):223–250.
5. Vinje WE, Gallant JL. Sparse coding and decorrelation in primary visual cortex during natural vision. *Science*. 2000;287(5456):1273–1276.
6. Williamson RS, Sahani M, Pillow JW. The equivalence of information-theoretic and likelihood-based methods for neural dimensionality reduction. 2013;.
7. Vu VQ, Ravikumar P, Naselaris T, Kay KN, Gallant JL, Yu B. Encoding and Decoding V1 fMRI Responses to Natural Images with Sparse Nonparametric Models. *Ann Appl Stat*. 2011;5(2B):1159–1182.
8. Huth AG, Nishimoto S, Vu AT, Gallant JL. A continuous semantic space describes the representation of thousands of object and action categories across the human brain. *Neuron*. 2012;76(6):1210–1224.
9. Stansbury DE, Naselaris T, Gallant JL. Natural scene statistics account for the representation of scene categories in human visual cortex. *Neuron*. 2013;79(5):1025–1034.
10. Pillow JW, Shlens J, Paninski L, Sher A, Litke AM, Chichilnisky EJ, et al. Spatio-temporal correlations and visual signalling in a complete neuronal population. *Nature*. 2008;454(7207):995–999.
11. Vogelstein JT, Watson BO, Packer AM, Yuste R, Jedynak B, Paninski L. Spike inference from calcium imaging using sequential Monte Carlo methods. *Biophys J*. 2009;97(2):636–655.
12. Park IM, Meister MLR, Huk AC, Pillow JW. Encoding and decoding in parietal cortex during sensorimotor decision-making. *Nat Neurosci*. 2014;17(10):1395–1403.
13. Buesing L, Machado TA, Cunningham JP, Paninski L. Clustered factor analysis of multineuronal spike data. In: Ghahramani Z, Welling M, Cortes C, Lawrence ND, Weinberger KQ, editors. *Advances in Neural Information Processing Systems 27*. Curran Associates, Inc.; 2014. p. 3500–3508.
14. Archer E, Park IM, Buesing L, Cunningham J, Paninski L. Black box variational inference for state space models. 2015;.
15. Zhao Y, Park IM. Variational Latent Gaussian Process for Recovering Single-Trial Dynamics from Population Spike Trains. 2016;.
16. Gao Y, Archer E, Paninski L, Cunningham JP. Linear dynamical neural population models through nonlinear embeddings. 2016;.

17. Ulrich KR, Carlson DE, Lian W, Borg JS, Dzirasa K, Carin L. Analysis of Brain States from Multi-Region LFP Time-Series. In: Ghahramani Z, Welling M, Cortes C, Lawrence ND, Weinberger KQ, editors. *Advances in Neural Information Processing Systems 27*. Curran Associates, Inc.; 2014. p. 2483–2491.
18. Putzky P, Franzen F, Bassetto G, Macke JH. A Bayesian model for identifying hierarchically organised states in neural population activity. In: Ghahramani Z, Welling M, Cortes C, Lawrence ND, Weinberger KQ, editors. *Advances in Neural Information Processing Systems 27*. Curran Associates, Inc.; 2014. p. 3095–3103.
19. Wainwright MJ, Jordan MI. Graphical Models, Exponential Families, and Variational Inference. *Found Trends Mach Learn*. 2008;1(1-2):1–305.
20. Ghahramani Z, Jordan MI. Factorial hidden Markov models. *Machine learning*. 1997;29(2-3):245–273.
21. Abramowitz M, Stegun IA. *Handbook of mathematical functions: with formulas, graphs, and mathematical tables*. 55. Courier Corporation; 1964.
22. Beal MJ. *Variational algorithms for approximate Bayesian inference*. University of London; 2003.
23. Roitman JD, Shadlen MN. Response of neurons in the lateral intraparietal area during a combined visual discrimination reaction time task. *The Journal of neuroscience*. 2002;22(21):9475–9489.
24. Latimer KW, Yates JL, Meister MLR, Huk AC, Pillow JW. Single-trial spike trains in parietal cortex reveal discrete steps during decision-making. *Science*. 2015;349(6244):184–187.
25. McMahon DBT, Jones AP, Bondar IV, Leopold DA. Face-selective neurons maintain consistent visual responses across months. *Proc Natl Acad Sci U S A*. 2014;111(22):8251–8256.
26. McMahon DBT, Russ BE, Elnaiem HD, Kurnikova AI, Leopold DA. Single-Unit Activity during Natural Vision: Diversity, Consistency, and Spatial Sensitivity among AF Face Patch Neurons. *Journal of Neuroscience*. 2015;35(14):5537–5548. doi:10.1523/JNEUROSCI.3825-14.2015.
27. Perrett DI, Hietanen JK, Oram MW, Benson PJ, Rolls ET. Organization and Functions of Cells Responsive to Faces in the Temporal Cortex [and Discussion]. *Philosophical Transactions of the Royal Society of London B: Biological Sciences*. 1992;335(1273):23–30. doi:10.1098/rstb.1992.0003.
28. Freiwald WA, Tsao DY. Functional Compartmentalization and Viewpoint Generalization Within the Macaque Face-Processing System. *Science*. 2010;330(6005):845–851. doi:10.1126/science.1194908.
29. Yu SZ, Kobayashi H. Practical implementation of an efficient forward-backward algorithm for an explicit-duration hidden Markov model. *Signal Processing, IEEE Transactions on*. 2006;54(5):1947–1951.

30. Blei DM, Jordan MI. Variational inference for Dirichlet process mixtures. *Bayesian Anal.* 2006;1(1):121–143.
31. Mitchell CD, Jamieson LH. Modeling Duration in a Hidden Markov Model with the Exponential Family. In: *Acoustics, Speech, and Signal Processing*; 1993.
32. Mitchell C, Harper M, Jamieson L. On the complexity of explicit duration HMM's. *IEEE Trans Audio Speech Lang Processing.* 1995;3(3):213–217.

Supplementary Information 1

Mathematical derivation for ELBO and Inference

1 Evidence Lower Bound (ELBO)

Here we derive the evidence lower bound (ELBO) used as a variational objective by our inference algorithm. That is, we want to calculate

$$\mathcal{L} \equiv \mathbb{E}_q \left[\log \frac{p(\Theta|N)}{q(\Theta)} \right] = \mathbb{E}_q [\log p(\Theta|N)] + \mathcal{H}[q(\Theta)] \quad (17)$$

From [22], this can be written

$$\begin{aligned} \mathcal{L} = \mathbb{E}_{q(\pi)} \left[\log \frac{p(\pi)}{q(\pi)} \right] &+ \mathbb{E}_{q(A)} \left[\log \frac{p(A)}{q(A)} \right] + \mathbb{E}_q \left[\log \frac{p(N, z|\lambda, A, \pi)}{q(z)} \right] \\ &+ \mathbb{E}_{q(\theta)} \left[\log \frac{p(\theta)}{q(\theta)} \right] + \mathbb{E}_{q(\lambda)} \left[\log \frac{p(\lambda)}{q(\lambda)} \right] + \mathbb{E}_{q(\gamma)} \left[\log \frac{p(\gamma)}{q(\gamma)} \right] \end{aligned} \quad (18)$$

For the first two terms, updates are standard and covered in [22]. The rest we do piece-by-piece below:

1.1 Log evidence

We would like to calculate $\mathbb{E}_q \left[\log \frac{p(N, z|x, \Theta)}{q(z)} \right]$. To do this, we make use of expectations calculated via the posteriors returned from the forward-backward algorithm

$$\xi_t \equiv p(z_t|N, \theta) \quad \Xi_{t,ij} \equiv p(z_{t+1} = j, z_t = i|N, \theta) \quad \log Z_t = \log p(N_{t+1}|N_t, \Theta) \quad (19)$$

Here, we have suppressed the latent feature index k and abuse notation by writing the observation index as t , but in the case of multiple observations at a given time, we pool across units and presentations: $N_t \equiv \sum_{m;t(m)=t} N_m$. From this, we can write

$$\begin{aligned} \mathbb{E}_q [\log p(N, z|x, \Theta)] &= \sum_{mkr} [N_m (\overline{\log \theta_m} + \overline{\log \lambda_{0u(m)}} + \xi_{t(m)k} \overline{\log \lambda_{zuk}} + x_{t(m)r} \overline{\log \lambda_{xu(m)r}})] \\ &- \sum_m \overline{\theta_m} \mathbb{E}_q [\Lambda_{t(m)u(m)}] + \sum_{tk} \left[\text{tr} \left(\Xi_{tk} \overline{\log A_k^T} \right) + \xi_{0k}^T \overline{\log \pi_k} \right] + \text{constant} \end{aligned} \quad (20)$$

In what follows, we will drop the irrelevant constant. For $\overline{\log y}$, where $y \in \{\theta, \lambda_0, \lambda_z, \lambda_x\}$, the assumption $q(y) = \text{Ga}(\alpha, \beta)$ gives

$$\overline{\log y} = \psi(\alpha) - \log \beta \quad (21)$$

with $\psi(x)$ the digamma function. Likewise, the expectation $\bar{\theta}$ is straightforward. For the expectation of the rate, we have

$$\mathbb{E}_q \left[\lambda_{0u} \prod_k (\lambda_{zuk})^{z_{tk}} \prod_r (\lambda_{xur})^{x_{tr}} \right] = \frac{\alpha_{0u}}{\beta_{0u}} \prod_k \left(1 - \xi_{tk} + \xi_{tk} \frac{\alpha_{zuk}}{\beta_{zuk}} \right) \prod_r \frac{1}{\beta_{xur}^{x_{tr}}} \frac{\Gamma(\alpha_{xur} + x_{tr})}{\Gamma(\alpha_{xur})} \quad (22)$$

However, for $\alpha \gg x$, we have $\Gamma(\alpha + x)/\Gamma(\alpha) \approx \alpha^x$, so that we can write

$$\mathbb{E}_q[\Lambda_{tu}] = H_{0u} F_{tu} G_{tu} \quad (23)$$

with $G_{tu} \approx \prod_r (\alpha_{xur}/\beta_{xur})^{x_{tr}}$. In addition, it will later be useful to have the expectation over *all except* a particular feature k or r , for which we define

$$F_{tuk} \equiv \prod_{k' \neq k} \left(1 - \xi_{tk'} + \xi_{tk'} \frac{\alpha_{zuk'}}{\beta_{zuk'}} \right) \quad (24)$$

$$G_{tur} \equiv \prod_{r' \neq r} \left(\frac{\alpha_{xur'}}{\beta_{xur'}} \right)^{x_{tr'}} \quad (25)$$

Finally, we want the entropy of the variational posterior over z , $\mathbb{E}_q[-\log q(z)]$. We can write this in the form

$$- \sum_{tk} \left[\xi_{tk}^T \eta_{tk} + \text{tr} \left(\Xi_{tk} \tilde{A}_k^T \right) + \xi_{0k}^T \tilde{\pi}_k - \log Z_{tk} \right] \quad (26)$$

with $(\eta, \tilde{A}, \tilde{\pi})$ the parameters of the variational posterior corresponding to the emission, transition, and initial state probabilities of the Markov chain (interpreted as matrices) and Z the normalization constant. From [22], we have that variational updates should give

$$\tilde{A}_k \leftarrow \overline{\log A_k} \quad \tilde{\pi}_k \leftarrow \overline{\log \pi_k} \quad (27)$$

while the effective emission probabilities in the ‘‘on’’ ($z = 1$) state of the HMM are

$$\eta_{tk} \leftarrow \delta_{z_{tk},1} \sum_{m;t(m)=t} N_m \overline{\log \lambda_{zu(m)k}} - \sum_{m;t(m)=t} \overline{\theta}_m H_{0u(m)} F_{tku(m)} G_{tu(m)} \quad (28)$$

Given these update rules, we can then alternate between calculating $(\eta, \tilde{A}, \tilde{\pi})$, performing forward-backward to get $(\xi, \Xi, \log Z)$ and recalculating $(\eta, \tilde{A}, \tilde{\pi})$.

1.2 Overdispersion, firing rate effects

Both the case of $p(\theta)$ and $p(\lambda)$ are straightforward. If we ignore subscripts and write $p(y) = \text{Ga}(a, b)$, $q(y) = \text{Ga}(\alpha, \beta)$, then

$$\mathbb{E}_q \left[\log \frac{p(y)}{q(y)} \right] = (\bar{a} - 1) \overline{\log y} + \bar{b} \bar{y} + \mathcal{H}[q(y)] \quad (29)$$

where again, $\overline{\log y}$, \bar{y} and $\mathcal{H}[q(y)]$ are straightforward properties of the Gamma distribution. Expectations of the prior parameters are listed in Table 1. Note in the last line that there is no expectation, since we have not assumed a hierarchy over firing rate effects for the covariates, x .

Table 1. Expectations of prior parameters for overdispersion and firing rates

Variable	$\mathbb{E}_q[a]$	$\mathbb{E}_q[b]$
θ	\bar{s}	\bar{s}
λ_0	\bar{c}_0	$\frac{c_0 d_0}{\bar{s}}$
λ_z	\bar{c}_z	$\frac{c_z d_z}{\bar{s}}$
λ_x	a_x	b_x

1.3 Hyperparameters

As shown in the main text, the hyperparameters c and d , given gamma priors, have conjugate gamma posteriors, so that their contribution to the evidence lower bound, $\mathbb{E}_q \left[\log \frac{p(\gamma)}{q(\gamma)} \right]$ is a sum of terms of the form

$$(a_c - 1) \overline{\log c} + b_c \bar{c} + \mathcal{H}[q(c)] + (a_d - 1) \overline{\log d} + b_d \bar{d} + \mathcal{H}[q(d)] \quad (30)$$

In other words, these are straightforward gamma expectations, functions of the prior parameters a and b for each variable and the corresponding posterior parameters α and β . Similarly, the overdispersion terms are exactly the same with the substitutions $c \rightarrow s$, $d \rightarrow 1$.

As we will see below, the expectations under the variational posterior of s , c , and d are themselves straightforward to calculate.

1.4 Autocorrelated noise

In the main text, we assumed the θ_m to be uncorrelated. However, it is possible to model temporal autocorrelation among the θ_m when observations correspond to the same neuron at successive time points. More specifically, let us replace the observation index m by τ , the experimental clock time. We then write a particular observation as corresponding to a stimulus time $t(\tau)$ and a set of units $u(\tau)$, which, for simplicity, we will assume fixed and simply write as u .³ To model the autocorrelation of noise across successive times, we then write

$$N_m \sim \text{Pois}(\Lambda_{t(\tau),u} \theta_{\tau u}) \quad \text{Assuming } \theta_{\tau u} = \phi_{\tau u} \theta_{\tau-1,u} \quad (31)$$

If $\phi_{0u} = \theta_{0u}$, we then have $\theta_{\tau u} = \prod_{\tau' \leq \tau} \phi_{\tau' u}$. In essence, this is a log-autoregressive process in which the innovations are not necessarily normally distributed. In fact, if we further assume that $p(\phi_{\tau u}) = \text{Ga}(s_u, r_u)$ and $q(\phi_{\tau u}) = \text{Ga}(\omega_{\tau u}, \zeta_{\tau u})$, we can once again make use of conjugate updates.

Given these assumptions, we need to make the following modifications for the third and fifth terms in the evidence lower bound of Eq (20):

$$\sum_{mkr} N_m \xi_{t(m)k} \overline{\log \lambda_{zuk}} \rightarrow \sum_{mkr} N_m \xi_{t(m)k} \overline{\log \lambda_{zuk}} + \sum_{\tau u} \overline{\log \phi_{\tau u}} \sum_{\tau' \geq \tau} N_{\tau' u} \quad (32)$$

$$- \sum_m \bar{\theta}_m \mathbb{E}_q [\Lambda_{t(m)u(m)}] \rightarrow - \sum_{\tau u} H_{0u} F_{\tau ku} G_{\tau u} \prod_{\tau' \leq \tau} \frac{\omega_{\tau' u}}{\zeta_{\tau' u}} \quad (33)$$

³The generalization to partially overlapping neurons and stimuli is straightforward but complex and notationally cumbersome.

Thus the effective emission probabilities in State 1 now become:

$$\eta_{tk} \rightarrow \delta_{z_{tk},1} \sum_m N_m \overline{\log \lambda_{zuk}} - \sum_{u;t(\tau)=t} H_{0u} F_{\tau ku} G_{\tau u} \prod_{\tau' \leq \tau} \frac{\omega_{\tau' u}}{\zeta_{\tau' u}} \quad (34)$$

1.5 Latent states, semi-Markov dynamics

We model each of the latent states z_{tk} as an independent Markov process for each feature k . That is, each k indexes an independent Markov chain with initial state probability $\pi_k \sim \text{Dir}(\alpha_\pi)$ and transition matrix $A_k \sim \text{Dir}(\alpha_A)$. For the semi-Markov case, we assume that the dwell times in each state are distributed independently for each chain according to an integer-valued, truncated lognormal distribution with support on the integers $1 \dots D$:

$$p_k(d|z=j) = \text{Log-Normal}(d|m_{jk}, s_{jk}^2)/W_{jk} \quad (35)$$

$$W_{jk} = \sum_{d=1}^D \text{Log-Normal}(d|m_{jk}, s_{jk}^2) \quad (36)$$

Note that we have allowed the dwell time distribution to depend on both the feature k and the state of the Markov chain j . In addition, we put independent Normal-Gamma priors on the mean (m_{kj}) and precision ($\tau_{kj} \equiv s_{kj}^{-2}$) parameters of the distribution: $(m, \tau) \sim \text{NG}(\mu, \lambda, \alpha, \beta)$.

In this case, we additionally need to perform inference on the parameters (m, τ) of the dwell time distributions for each state. In the case of continuous dwell times, our model in Equation 35 would have $W = 1$ and be conjugate to the Normal-Gamma prior on (m, τ) , but the restriction to discrete dwell times requires us to again lower bound the variational objective:

$$\mathbb{E}_q[-\log W_{jk}] = \mathbb{E}_q \left[-\log \left(\sum_{d=1}^D p(d|j) \right) \right] \geq -\log \sum_{d=1}^D \mathbb{E}_q[p(d|j)] \quad (37)$$

This correction for truncation must then be added to $\mathbb{E}_q[p(z|\Theta)]$. For inference in the semi-Markov case, we use an extension of the forward-backward algorithm [29], at the expense of computational complexity $\mathcal{O}(SDT)$ ($S = 2$) per latent state, to calculate $q(z_k)$. For the 4SK hyperparameters of the Normal-Gamma distribution, we perform an explicit BFGS optimization on the 4S parameters of each chain on each iteration (detailed in Subsection 2.2.2).

2 Inference

2.1 Conjugate updates

For updates on the overdispersion, firing rate, and hyperparameter variables, we have the simple conjugate update rules depicted in Table 2. These can be derived either from free-form variational arguments, or exponential family rules, but are in any case straightforward [30]. If we assume a $\text{Ga}(a, b)$ prior and $\text{Ga}(\alpha, \beta)$ variational posterior, all of these have a simple algebraic update in terms of sufficient statistics.

Here, we overload notation to write $N_{tu} = \sum_m \delta_{u(m),u} \delta_{t(m),t} N_m$, $\bar{\theta}_u = \sum_m \delta_{u(m),u} \bar{\theta}_m$, and make use of H , G , and F as defined in Eq (23) - (25). Indeed, our implementation

Table 2. Conjugate updates for Gamma distributions

Variable	$\alpha - a$	$\beta - b$
θ_m	N_m	$H_{0u(m)} F_{t(m)u(m)} \overline{G_{t(m)u(m)}}$
s_u	$\frac{1}{2} \sum_m \delta_{u(m),u}$	$\sum_m \delta_{u(m),u} [\overline{\theta}_m - \overline{\log \theta}_m - 1]$
λ_{0u}	$\sum_t N_{tu}$	$\overline{\theta}_u H_{0u} \sum_t F_{tu} G_{tu}$
λ_{zuk}	$\sum_t N_{tu} \xi_{tk}$	$\overline{\theta}_u H_{0u} \sum_t F_{tuk} G_{tu}$
λ_{xur}	$\sum_t N_{tu} x_{tr}$	cf. Section 2.2
c_0	$U/2$	$\sum_u \mathbb{E}_q [d_0 \lambda_{0u} - \log \lambda_{0u} - \log d_0 - 1]$
c_{zk}	$U/2$	$\sum_u \mathbb{E}_q [d_{zk} \lambda_{zuk} - \log \lambda_{zuk} - \log d_{zk} - 1]$
c_{xr}	$U/2$	$\sum_u \mathbb{E}_q [d_{xr} \lambda_{xur} - \log \lambda_{xur} - \log d_{xr} - 1]$
d_0	$U \mathbb{E}_q [c_0]$	$\sum_u \mathbb{E}_q [c_0 \lambda_{0u}]$
d_{zk}	$U \mathbb{E}_q [c_{zk}]$	$\sum_u \mathbb{E}_q [c_{zk} \lambda_{zuk}]$
d_{xr}	$U \mathbb{E}_q [c_{xr}]$	$\sum_u \mathbb{E}_q [c_{xr} \lambda_{xur}]$
ϕ_{ju} for $j \in \{1, \dots, \tau\}$	$\sum_{\tau' \geq j} N_{\tau'u}$	$\sum_{u, \tau \geq j} F_{t(\tau)} \prod_{\substack{\tau' \leq \tau \\ \tau' \neq j}} \frac{\omega_{\tau'u}}{\zeta_{\tau'u}}$

caches F and G for a substantial speedup (at the cost of additional memory requirements). For autocorrelated noise, the update rules are for the j -th item in the series of autocorrelation.

2.2 Non-conjugate updates

We employ explicit optimization steps for two updates in our iterative Algorithm 1. In each case, we employ an off-the-shelf optimization routine, though more efficient alternatives are likely possible.

2.2.1 Covariate firing rate effects

Because we do not restrict the covariates $x(t)$ to be binary, Equation 22 no longer yields a conditional log probability for λ_x in the exponential family. This leaves us with a transcendental equation to solve for β_{xr} . However, from Table 2, we see that $\alpha_{xr} \gg \sum_t x_{tr}$, allowing us to approximate $G_t \approx \prod_r (\alpha_{xr} / \beta_{xr})^{x_{tr}}$ as we have done above. Moreover, since the sum $\sum_t G_t \sim T \overline{G}$, we expect $\alpha_x / \beta_x \approx 1$ at the optimum for most reasonable datasets. We thus reparameterize $\beta_{xur} = \alpha_{xur} e^{-\epsilon_{ur}}$ and write the relevant ϵ -dependent piece of the objective function \mathcal{L} as

$$\mathcal{L}_\epsilon = \sum_{ur} [a_{xur} \epsilon_{ur} - b_{xur} e^{-\epsilon_{ur}}] - \sum_m \overline{\theta}_m H_{0u(m)} F_{t(m)u(m)} e^{-\sum_r \epsilon_{u(m)r} x_{t(m)u(m)r}} \quad (38)$$

We also supply the optimizer with the gradient:

$$\nabla_\epsilon \mathcal{L}_\epsilon = a_{xur} - b_{xur} e^{-\epsilon_{ur}} - \sum_{m; u(m)=u} x_{t(m)ur} \overline{\theta}_m H_{0u} F_{t(m)u} e^{-\sum_r \epsilon_{ur} x_{t(m)ur}} \quad (39)$$

where we sum only over observations with $u(m) = u$. On each iterate, we then optimize \mathcal{L}_ϵ , initializing β_x to the just-updated value of α_x . In addition, we do not update firing rate effects for covariates separately, but optimize β_{xur} for all r together. Again, more efficient schemes are no doubt possible.

2.2.2 Semi-Markov duration distribution

If the dwell time distributions of states in the semi-Markov model were truly continuous, the parameters (m, s^2) of a lognormal distribution $p(d|j)$ would have a Normal-Gamma conjugate prior, and updates would be closed-form. However, the requirement that the durations be integers and that there exist a maximal duration, D , over which these probability mass functions must normalize results in an extra term in $\mathbb{E}_q[\log p]$ arising from the normalization constant. In this case, we must explicitly optimize for the parameters of the Normal-Gamma prior on (m, s^2) . However, unlike the case of 2.2.1, these parameters are only updated for one latent feature at a time. Since the Normal-Gamma distribution has only 4 parameters and the number of states of the latent variable is $S = 2$, this requires updating $4SK$ parameters, but only taken $4S = 8$ at a time, a much more manageable task.

To derive the optimization objective, we begin by noting that the semi-Markov model adds to the terms involving Ξ and ξ_0 in latent state dynamics an additional piece:

$$\sum_{dj k} C(d, j, k) \mathbb{E}_q \left[\log p_k(d|j) - \log \left(\sum_{d=1}^D p_k(d|j) \right) \right] \geq \sum_{dj k} C(d, j, k) \left[\mathbb{E}_q [\log p_k(d|j)] - \log \sum_{d=1}^D \mathbb{E}_q [p_k(d|j)] \right] \quad (40)$$

where as noted above, the second term inside the expectation arises from the need to normalize $p(d|j)$ over discrete times and the inequality follows from Jensen's Inequality. Here, d is the duration variable, j labels states of the chain (here 0 and 1), and k , as elsewhere, labels chains [29,31,32]. C is defined for each state and chain as the probability of a dwell time d in state j *conditioned on* the event of just having transitioned to j ^{4 5}

Thus the objective to be optimized is

$$\sum_{dj k} C(d, j, k) \left[\mathbb{E}_q [\log p_k(d|j)] - \log \sum_{d=1}^D \mathbb{E}_q [p_k(d|j)] \right] + \mathbb{E}_q \left[\log \frac{p(m, \tau)}{q(m, \tau)} \right] \quad (42)$$

For the case of $p(d|m, s^2)$ Log-Normal and $(m, \tau = s^{-2})$ Normal-Gamma, the terms $\mathbb{E}_q[\log p(d)]$ involve only routine expectations of natural parameters of the Normal-Gamma, and similarly for the expected log prior and entropy in the last term. Only slightly more complicated is the term arising from the normalization constant, which in the standard $(\mu, \lambda, \alpha, \beta)$ parameterization of the Normal-Gamma takes the form

$$\mathbb{E}_q[p(d|m, \tau)] = \int d\tau dm p(d|i, m, \tau) q(m, \tau) = \frac{1}{\sqrt{2\pi}d} \sqrt{\frac{\lambda}{1+\lambda}} \frac{\Gamma(\alpha + 1/2)}{\Gamma(\alpha)} \frac{\beta^{-\frac{1}{2}}}{\hat{\beta}^{\alpha + \frac{1}{2}}} \quad (43)$$

⁴Thus C is equivalent to $\mathcal{D}_{t|T}$ in [29].

⁵ We also note that, just as the emission, transition, and initial state probabilities have their counterparts in variational parameters $(\eta, \tilde{A}, \tilde{\pi})$ in $q(z)$, so C is matched by a term $-\sum_{dj k} C(d, j, k) \nu_{dj k}$ in $\mathbb{E}_q[-\log q]$. And in analogy with the HMM case, variation with respect to ν gives

$$\nu_{dj k} = \mathbb{E}_q [\log p_k(d|j)] - \log \sum_{d=1}^D \mathbb{E}_q [p_k(d|j)], \quad (41)$$

implying that there are cancellations between $\log p(N, z|\Theta)$ and $\log q(z)$ in \mathcal{L} and care must be taken when calculating it [22].

with

$$\hat{\beta} \equiv 1 + \frac{1}{2\beta} \frac{\lambda}{1 + \lambda} (\log d - \mu)^2 \quad (44)$$

This can be derived either by performing the integral directly or by noting that the result should be proportional to the posterior (Normal-Gamma, by conjugacy) of (m, τ) after having observed a single data point, $\log d$.

Algorithm 1 Iterative update for variational inference

```

1: procedure ITERATE
2:   Update baselines  $\lambda_0$  ▷ conjugate Gamma
3:   Update baseline hyperparameters  $\gamma_0$  ▷ conjugate Gamma
4:   for  $k = 1 \dots K$  do
5:     Update firing rate effects  $\lambda_{zk}$  ▷ conjugate Gamma
6:     Update firing rate hyperparameters  $\gamma_{zk}$  ▷ conjugate Gamma
7:     Calculate expected log evidence  $\eta_k$ 
8:     Update Markov chain parameters  $\tilde{A}_k, \tilde{\pi}_k$ 
9:      $\xi_k, \Xi_k, \log Z_k \leftarrow$  FORWARD-BACKWARD( $\eta_k, \tilde{A}_k, \tilde{\pi}_k$ )
10:    if semi-Markov then
11:      Update duration distribution  $p_k(d|j)$  ▷ BFGS optimization
12:    end if
13:    Update cached  $F$ 
14:  end for
15:  Update covariate firing effects  $\lambda_x$  ▷ BFGS optimization
16:  Update cached  $G$ 
17:  Update overdispersion  $\theta$  ▷ conjugate Gamma
18: end procedure

```

3 Experiments

Code for all algorithms and analyses is available at <https://github.com/pearsonlab/spiketopics>.

Supplementary Information 2

Categorization of multinomial logistic regression

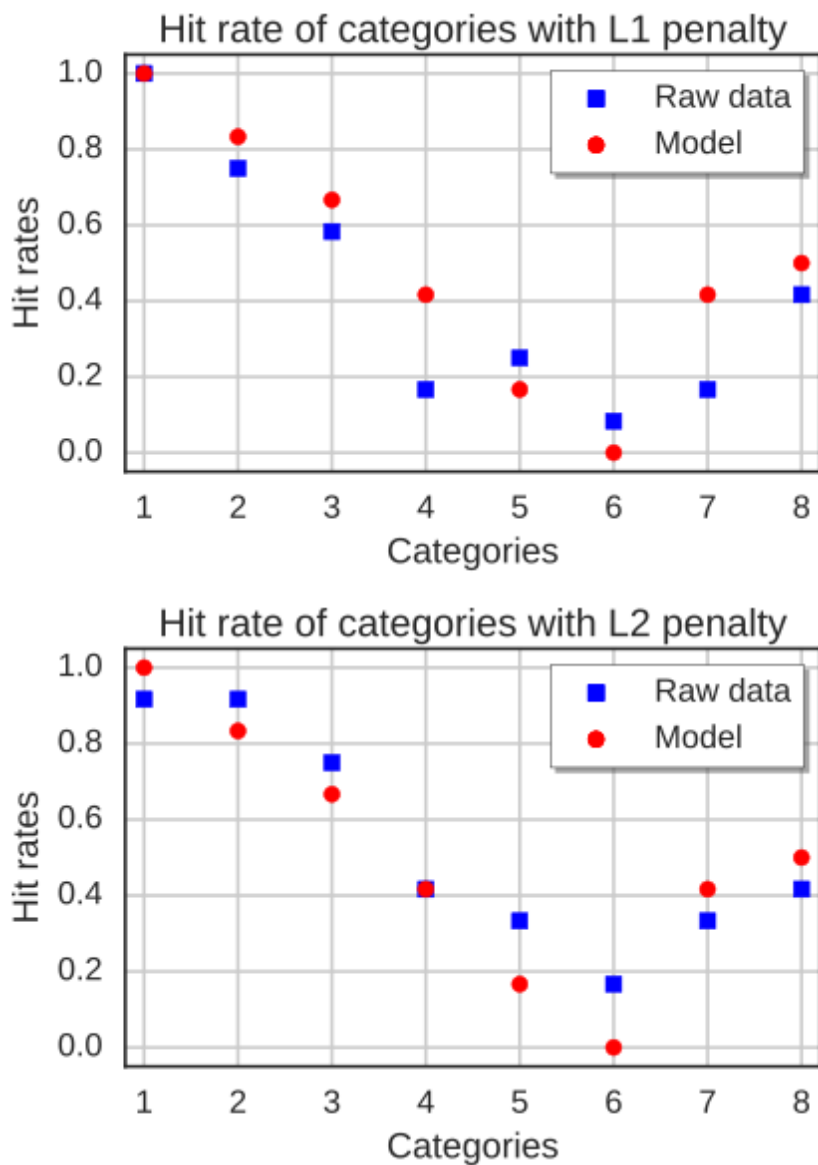


Fig 7. Hit rates within eight categories

Compare the hit rates of actual data and inferred states of the macaque dataset. A. Multinomial logistic regression using L1 regularization. Model inferred features outperform the raw data in 5/8 categories and tie in one category. Model wins. B. Multinomial logistic regression using L2 regularization. Model inferred features outperform 3/8 categories and tie in one. Both tied.